Title: Mild ultrasound-assisted synthesis of TiO_2 supported on magnetic nanocomposites for selective photo-oxidation of benzyl alcohol

Author: Juan C. Colmenares Weiyi Ouyang Manuel Ojeda Ewelina Kuna Olga Chernyayeva Dmytro Lisovytskiy Sudipta De Rafael Luque Alina M. Balu

PII: S0926-3373(15)30215-0
DOI: http://dx.doi.org/doi:10.1016/j.apcatb.2015.10.034
Reference: APCATB 14341

To appear in: *Applied Catalysis B: Environmental*

Received date: 3-9-2015
Revised date: 29-9-2015
Accepted date: 14-10-2015

Please cite this article as: Juan C.Colmenares, Weiyi Ouyang, Manuel Ojeda, Ewelina Kuna, Olga Chernyayeva, Dmytro Lisovytskiy, Sudipta De, Rafael Luque, Alina M.Balu, Mild ultrasound-assisted synthesis of TiO2 supported on magnetic nanocomposites for selective photo-oxidation of benzyl alcohol, Applied Catalysis B, Environmental http://dx.doi.org/10.1016/j.apcatb.2015.10.034

Mild ultrasound-assisted synthesis of TiO_2 supported on magnetic nanocomposites for selective photo-oxidation of benzyl alcohol

Juan C. Colmenares,[a]* Weiyi Ouyang[b], Manuel Ojeda[b], Ewelina Kuna[a], Olga Chernyayeva[a], Dmytro Lisovytskiy[a], Sudipta De[b], Rafael Luque[b] and Alina M. Balu[b]*

[a]*Institute of Physical Chemistry PAS, Kasprzaka 44/52, 01-224 Warsaw (Poland), E-mail: jcarloscolmenares@ichf.edu.pl*

[b]*Departamento de Quimica Organica, Universidad de Cordoba, Campus de Rabanales, Edificio Marie Curie, E-14014, Cordoba, Spain, E-Mail: go2balua@uco.es*

GRAPHICAL ABSTRACT

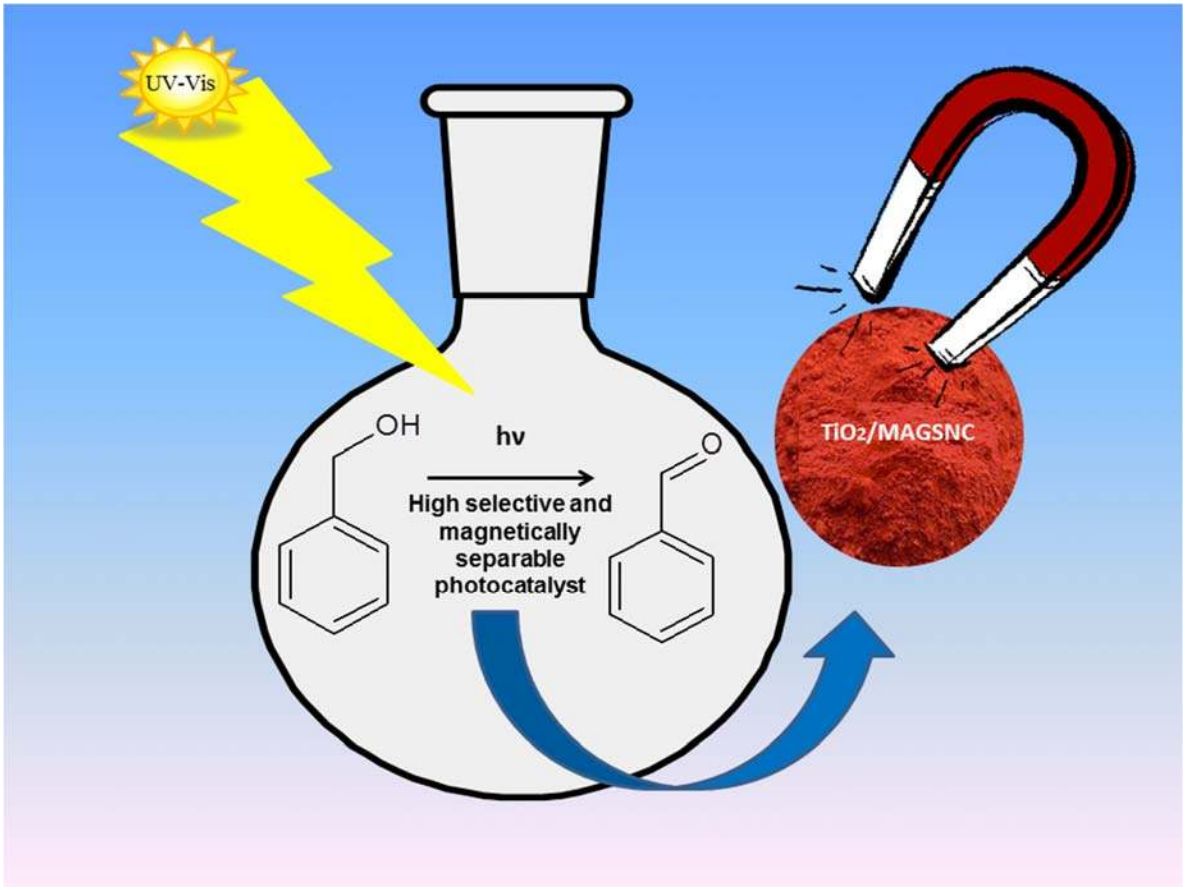

Highlights

- Simple synthesis of hybrid photocatalysts containing magnetic nanocomposites and titania.
- Selective and stable composite photocatalyst for liquid phase photocatalytic oxidation of benzyl alcohol.
- Sonication-based preparation of modern selective composite photocatalyst with magnetic properties for simple recovery.
- Advantages of combining magnetic filtration and photocatalysis for green chemistry synthesis.

Abstract

A simple and effective ultrasound-assisted wet impregnation method was developed for the preparation of magnetically separable TiO_2/maghemite-silica photo-active nanocomposites. The resulting nanomaterials were characterized by several techniques and subsequently tested for their photocatalytic activities in the liquid phase selective oxidation of benzyl alcohol. An unprecedented selectivity in organic media (90% in acetonitrile) towards benzaldehyde was achieved at a benzyl alcohol conversion of ca. 50%, being remarkably superior in terms of activity to any other supported transition metal catalysts reported to date as well as commercial titania Evonik P-25 photocatalyst.

Keywords: Selective photo-oxidation; Ultrasound-assisted impregnation; TiO_2; Aromatic alcohols; magnetic photocatalysts

Introduction

Photocatalysis is currently considered as one of the most advanced, environment friendly and promising technologies due to excellent merits such as clean, effective, energy-saving, and low cost.[1,2] Photocatalytic oxidation (PCO) could be a promising alternative of aforementioned chemical oxidation technologies for lignin oxidation in terms of selectivity and economic issues. In 1989, Ohnishi *et al.* studied the performance of different photocatalysts including ZnO, TiO_2, CdS, In_2O_3, WO_3, and Fe_2O_3 on lignin degradation.[3] Doping of noble metals such as Pt, Ag, and Au could further improved the efficiency of the photocatalyst. The next generation photocatalysts will be based on the utilization of a heterojunction between two photoactive materials with different band gap.[4]

Among various semiconductor photocatalysts used in the past 3 decades, TiO_2 received most attention due to its biological and chemical inertness, cost effectiveness, and the strong oxidizing power of the photogenerated holes.[5,6] However, one of the major problems of using pure TiO_2 is that only ultraviolet light photons can displace the valence band electrons of TiO_2 due to its high band-gap energy (3.2 eV), making only 5% of the solar radiation utilized. This problem can be solved by doping heteroatoms in the TiO_2 and creating new heterojunctions with TiO_2 materials that improve the photocatalytic properties of TiO_2 by enhancing the light absorption and delaying recombination of photogenerated electron–hole pairs.[7]

Selective oxidation of alcohols to their corresponding carbonyl compounds (especially aldehydes) is one of the important organic transformations as carbonyl compounds are widely used in food, beverages, and pharmaceutical industries, and as precursors in chemical industries.[8,9] The conversion of aromatic alcohols to aldehydes is particularly attractive since

aromatic alcohols represent themselves as model lignin compounds obtained after the depolymerization of lignin. The main purpose of studying these compounds is that they contain linkages that resemble those found in lignin and thus their reactivity could potentially provide insights into the degradation and reaction of the polymer structure as a whole.[10] Since benzyl alcohol is a key structural unit of most of lignin model compounds, major focus has been given to its reactivity and transformation strategies. Another advantage relates to the simplicity of benzyl alcohol as aromatic substrate and consequently possesses inferior analytical challenges relative to the complicated lignin models.

In recent years, the photo-assisted transformation of benzyl alcohol to benzaldehyde has attracted a great deal of attention as a potential alternative to effectively replace the industrial synthesis route *via* benzyl chloride hydrolysis derived from toluene chlorination or through toluene oxidation. Metal oxide based catalysts such as TiO_2,[11-13] Nb_2O_5,[14] and ZnO[15] have been well explored for the alcohol oxidation in presence of UV irradiation. Incorporation of various noble metals including Au,[16] Pd,[17] and Pt[18,19] on different photoactive catalyst supports has been reported to achieve improved activities even under visible light conditions. However, the use of noble metals is not suitable for the large scale transformation and in terms of practical implication. In this regard, composite materials consisting of transition metal oxides, carbon nitrides or graphene have shown a great deal of interests with nearly comparable activities.[20-22] Our group has recently designed Fe- and Cr-modified TiO_2 supported hybrid materials which have shown high selectivity in the oxidation of glucose to carboxylic acids.[23,24]

In continuation with research endeavors from our groups, herein we report a simple wet impregnation method coupled with ultrasonic irradiation for the preparation of TiO_2 supported onto maghemite-silica nanocomposites. The present method makes use of magnetically separable

supports previously described by our group (denoted as MAGSNC).[25] The unusual reaction conditions (extremely high temperatures and pressures form quickly in liquids due to acoustic cavitation phenomena) of the ultrasonic irradiation technique were key factors to achieve homogeneously impregnated materials with nanosized particles and the formation of heterojunctions between titania and the magnetic support. The catalysts were found to be highly photocatalytically active towards the selective oxidation of benzyl alcohol in both organic and aqueous environment. One of the major advantages of the materials also relies on the fact that the materials can be easily separated by using magnetic force for the next catalytic run.

Experimental

Photocatalysts preparation

25 wt% TiO_2/MAGSNC (maghemite-silica nanocomposites) was prepared as catalyst in the present work. Titania was supported on MAGSNC by a simple and mild ultrasound-assisted wet impregnation method.[26] MAGSNC powders (500 mg) were added into a solution of titanium tetra-isopropoxide TTIP (0.47 mL; 1.5 mmol) in isopropanol (total volume ratio of TTIP : isopropanol was 1:40) and the whole mixture was sonicated for 1 h (ultrasonic bath, frequency 35 kHz, 560 W, Sonorex Digitec-RC, Bandelin). The solvent was removed using a rotary evaporator without sonication (for the first 15 min) and then assisted by sonication increasing temperature to 50 °C. The final material was further dried for 3 h at 110 °C and subsequently calcined in a furnace at 400 °C (heating rate of 3 °C/min) for 5 h in an oxygen deficient atmosphere (static air).

Photocatalysts characterization

UV–Vis diffuse reflectance spectra were recorded on UV/VIS/NIR spectrophotometer Jasco V-570 equipped with an integrating sphere. The baseline was recorded using Spectralon™ poly(tetrafluoroethylene) as a reference material. To determine the band gap function, the Kubelka-Munk method based on the diffuse reflectance spectra was employed. The E_g was calculated form $(f(R)h\nu)^{1/2}$ versus hν plots. The function f(R) was calculated from the following equation:[27]

$$f(R) = \frac{(1-R)^2}{2R}$$

Powder XRD measurements were performed employing Bragg-Brentano configuration. This type of arrangement was provided using PANalytical Empyrean diffraction platform, powered at 40 kV × 40 mA and equipped with a vertical goniometer, with theta-theta geometry using Ni filtered Cu Kα radiation. Data were collected in range of 2θ = 5–120°, with step size of 0.008° and counting time 500 second per step.

XPS measurements were performed using a VG Scientific photoelectron spectrometer ESCALAB-210 using Al Kα radiation (1486.6 eV) from an X-ray source operating at 15 kV and 20 mA. Survey spectra were recorded for all the samples in the energy range from 0 to 1350 eV with 0.4 eV step. High resolution spectra were recorded with 0.1 eV step, 100 ms dwell time and 25 eV pass energy. Ninety degrees take-off angle was used in all measurements. The curve fitting was performed using the AVANTAGE software provided by Thermo Electron, which describes each component of the complex envelope as a Gaussian–Lorentzian sum function; a constant 0.3(±0.05) G/L ratio was used. The background was fitted using nonlinear Shirley

model. Scofield sensitivity factors and measured transmission function were used for quantification. Aromatic carbon C 1s peak at 284.5 eV was used as reference of binding energy.

Specific surface areas, pore volumes and average pore diameters were determined by N_2 physisorption using a Micromeritics ASAP 2020 automated system and the Brunauer–Emmet–Teller (BET) and the Barret–Joyner–Halenda (BJH) methods. Samples were degassed under vacuum (0.1 Pa) for 4 h at 300 °C prior to adsorption measurements.

Photocatalytic experiments

All reaction were carried out in a Pyrex cylindrical double-walled immersion well reactor equipped with medium pressure 125 W mercury lamp (λ = 365 nm), supplied by Photochemical Reactors Ltd. UK (Model RQ 3010). The bath reactor was stirred magnetically (1100 rpm) to obtain a homogenous suspension of the catalyst. The reaction temperature was established at 30 °C. Benzyl alcohol (1.5 mM, optimized concentration) was dissolved either in acetonitrile medium or in Milli-Q water. Experiments were performed from 150 mL of the mother solution and 1 g/L of catalyst concentration for 4 h under UV-light and air bubbling conditions (25 mL/min) (all conditions after optimization, results not shown). In order to equilibrate the adsorption-desorption over the photocatalyst surface, the reaction solution was left in the dark for 30 min before each reaction. Approx. 1 ml samples were collected directly from the photoreactor at specific time intervals and filtered (0.20 µm, 25 mm, nylon filters). The concentration of model compound was determined by a high performance liquid chromatography (HPLC, Waters Model 590 pump) equipped with a Dual Absorbance Detector (Waters 2487) and the SunFire™ C18 (3.5 µm, 150 mm length, 4.6 mm inner diameter) column provided by Waters. The mobile

phase was Milli-Q water/acetonitrile/methanol in the volumetric ratio of 77.5 : 20 : 2.5 with 0.1% of H_3PO_4. We used isocratic elution at a flow rate of 1 mL/min. The injection volume was 10 μL.

Results and discussion

X-ray diffraction (XRD) patterns of synthesized magnetic nanocomposites clearly confirmed the presence of anatase (TiO_2) and maghemite phases (γ-Fe_2O_3) in the material (Fig. 1). A similar XRD pattern could be in principle associated to magnetite (Fe_3O_4; it is challenging to distinguish these clearly by XRD), but the absence of Fe^{2+} surface species (XPS Fig. 2) and the reddish-like color are consistent with a maghemite magnetic phase as previously reported.[28] An average maghemite nanoparticle (NP) diameter of 5.8 nm and anatase TiO_2 of ca. 4 nm could be worked out from the (311) and (101) diffraction line, respectively, using the Scherrer equation.

X-ray photoelectron spectroscopy (XPS) analysis of the magnetic photoactive nanocomposites confirmed the presence of TiO_2 (458.8 eV) as well as the exclusive presence of Fe^{3+} (710.8 eV, from the maghemite phase) in both MAGSNC and TiO_2/MAGSNC upon calcination of the materials at 400 °C (Fig. 2). Fe^0 species, from the action of hydrogen radicals during sonication may have been formed during the composite preparation. Further thermal treatment in static air at 400 °C oxidized all Fe species towards the observed maghemite phase. The magnetic phase was found to be well preserved even after calcination at 400 °C, despite the hematite phase being most thermodynamically stable at temperatures over 300 °C.[28]

Textural properties of MAGSNC and TiO_2-MAGSNC were evaluated by N_2 sorption isotherms, showing a characteristic type IV isotherm profile of mesoporous materials (results not shown). A significant deterioration in textural properties was observed upon formation of the magnetic TiO_2-functionalized material (Table 1). Surface area as well as pore volume remarkably decreased with respect to MAGSNC. Pore volumes were reduced from 0.51 to 0.31 mL g^{-1}, most probably related to the pore deposition of titania in the materials under ultrasound irradiation. ICP analysis of TiO_2-MAGSNC showed an actual content of TiO2 close to 25%, in good agreement with theoretical Ti loadings.

The optical properties of the synthesized photocatalyst were studied by diffuse reflectance (DR) UV-Vis spectroscopy (Table 1, Figure 3). Figure 3 represents the DR UV-Vis absorption spectra of all tested photocatalysts. In general, commercially available Evonik TiO_2 P25 (photocatalytic standard) shows an absorption edge at around 394 nm and no absorption in visible region above 400 nm (Table 1, Fig. 3).[26] DR UV-Vis spectra (Fig. 3) of our presently reported samples showed a red shift of the absorption band into the visible region and a significant enhancement of light absorption at a wavelength of around 700 nm as compared to TiO_2 P25. This absorption in the visible range can be certainly induced by γ-Fe_2O_3 maghemite (the main component of the photocatalytic composite).

Based on Kubelka–Munk function, the calculated band gap of MAGSNC and TiO_2/MAGSNC catalysts were found to be 1.75 and 1.78 eV respectively (Table 1). It was very difficult to measure titania band gap due to the strong support (MAGSNC) absorption in the visible range. We believe, partially based on DR UV-Vis spectra (Fig. 3) and photocatalytic

tests, that the difficulties to observe the absorption of TiO_2 in the composite (25 wt%TiO_2/MAGSNC) is probably caused by the close interfacial interactions (formation of spatially well-organized semiconductor phases heterojuctions) between anatase and maghemite phases formed as a result of acoustic cavitation effect during the material synthesis. The significant absorption of visible light of TiO_2 in the composite TiO_2/MAGSNC material (as compared to TiO_2 P25 which exclusively absorbs UV irradiation with a band gap value of 3.15 eV) could be attributed to the localized states near the conduction or valence band of the modified semiconductor.[29] Amongst a variety of transitional metal dopants, a maghemite phase was selected as support due to the fact that Fe^{3+} can provide a shallow trap for photogenerated electron and holes because the energy level of Fe^{2+}/Fe^{3+} lies close to that of Ti^{3+}/Ti^{4+}, favoring the separation of photo-generated electron-hole pairs. These consequently result in the improvement of photocatalytic performance. Furthermore, the radius of Fe^{3+} (0.64 Å) is almost similar to that of Ti^{4+} (0.68 Å),[30] and therefore a co-catalytical amount of Fe^{3+} might be easily incorporated from the support (maghemite-silica nanocomposite) into the crystal lattice of TiO_2 during the synthesis under sonication.

We do believe that during titania incorporation on MAGSNC support under ultrasonic treatment (the action of shock waves and high-velocity microjet impact under acoustic cavitation conditions)[31] Fe^{3+} could migrate from the support and replace part of Ti^{4+} ions during the impregnation process. We were unable to visualise any shift in the XRD anatase signal due to the high dispersion and the very small amount of Ti incorporated into the material. Additionally, the formation of heterostructures (heterojunctions) between TiO_2 and γ-Fe_2O_3 is also possible and they can spatially separate the charge carriers potentially increasing the photoactivity of the materials as described in the photoconversion of benzyl alcohol.

A model photo-oxidation reaction of a simple aromatic alcohol (benzyl alcohol) was selected to study the effectiveness of the prepared TiO_2/MAGSNC photonanocomposite.

The controlled photolysis reaction (without catalysts) provided negligible conversion (<5%) of benzyl alcohol after 4 h of illumination time (Table 2), similar to that obtained under dark conditions (no conversion). The use of MAGSNC support as catalyst also provided very low conversion of benzyl alcohol which indicates that γ-Fe_2O_3 itself has no significant activity towards photo-oxidation process (Table 2). Main drawbacks of using bare iron oxides as photocatalysts relate to the fact they can promote the electron-hole recombination giving inactive materials.[32] In contrast, the combination TiO_2/MAGSNC as photocatalyst in acetonitrile medium significantly improved the conversion (up to 48%) with an unprecedented benzaldehyde selectivity of 90% achieved under photocatalytic conversion conditions. Selectivity to benzaldehyde reached a maximum of 98% after an illumination time of 2 h (ca. 30% conversion).

A maximum yield of benzaldehyde (47%) could be achieved with the unprecedented >90% selectivity which to the best of our knowledge constitutes one of the best reported results of benzyl alcohol oxidation under photocatalytic conditions. More interestingly, no over-oxidation products (such as benzoic acid and CO_2, observed in considerable quantities for TiO_2 P-25 Evonik) were observed for TiO_2/MAGSNC under the investigated reaction conditions.

The same reaction in aqueous medium resulted very low conversion (5%) with low benzaldehyde selectivity. A crucial role of solvents in the photocatalytic oxidation process was also observed in our previous reports and by other authors.[23,24,33] The addition of acetonitrile in various photocatalytic reactions has been reported to improve selectivity to target products due to

the "*shield effect*" provided by certain solvents (i.e. acetonitrile).[33] In the photoredox process, acetonitrile was proved to act as a weak base that stabilizes reaction products via solvation, inhibiting proton transfer and at the same time preventing the formation of radical species that afford undesirable oxidation side products.[34]

Incorporation of 25 wt% TiO_2 on the surface of MAGSNC was believed to form a close heterojunction of two semiconductors (TiO_2/γ-Fe_2O_3) favoring the electron transfer from γ-Fe_2O_3 (Eg = 1.78 eV) to TiO_2 (photosensitization of titania) and making it more photoselective as compared to TiO_2 P-25 (90% and 32% selectivity towards benzaldehyde, respectively, Table 2) with a good benzyl alcohol conversion (ca. 50%). Additionally, the nanophotocatalyst was proved to be highly stable under the investigated reaction conditions, with no leaching of Fe or Ti after several hours of reaction (undetected by ICP/MS).

An increase in the crystallite size of TiO_2 materials produces decreased selectivity in the photo-oxidation process.[35] Highly crystalline materials possess lower surface areas due to which the surface hydroxyl group density decreases and consequently result lower activity. Our photoactive nanocomposite material possessed a high surface area (292 m^2g^{-1}, Table 1), and its TiO_2 component has very small crystallite size of approx. 4 nm and exclusively composed of anatase phase (Fig. 1). The adsorptive affinity of rutile for organic compounds (e.g. benzyl alcohol) is lower to that of anatase and rutile exhibits higher rates of recombination electron–hole (lower photo-catalytic activity) in comparison to anatase.[36]

Conclusions

Magnetically separable TiO_2/MAGSNC photocatalysts were synthesized following the improved wet impregnation method assisted by ultrasonic irradiation. The spatially ordered heterojuntion between TiO_2 and γ-Fe_2O_3 and a potential co-catalytic incorporation of Fe^{3+} (from the support MAGSNC) into the titania structure might significantly increase the sensitization and decreased the band gap energy of TiO_2, effectively improving the photocatalytic activity and selectivity of the materials towards selective oxidation of benzyl alcohol to benzaldehyde. Solvents played a significant role in the photo-oxidation process with materials showed very good conversion and selectivity in acetonitrile but not in aqueous conditions. This work provided a simple low-cost preparation of magnetically separable titania supported photocatalysts for the selective oxidation of aromatic alcohols which has a promising potential in future studies towards the photochemical conversion of phenolic-type compounds.

Acknowledgements

Prof. Colmenares would like to thank the Institute of Physical Chemistry of the Polish Academy of Sciences for all support. Rafael Luque gratefully acknowledges Spanish MICINN for financial support via the concession of a RyC contract (ref: RYC-2009-04199) and funding under project CTQ2011-28954-C02-02 (MEC). Consejeria de Ciencia e Innovacion, Junta de Andalucia is also gratefully acknowledged for funding project P10-FQM-6711. JCC, AMB and RL gratefully acknowledge support from COST Action FP1306 for networking and possibilities for meetings and future students exchange.

Reference

1.X. Lang, X. Chen, J. Zhao, Chem. Soc. Rev. 43 (2014) 473–486.

2J.C. Colmenares, R. Luque, Chem. Soc. Rev. 43 (2014) 765–778.

3 H. Ohnishi, M. Matsumura, H. Tsubomura, M. Iwasaki, Ind. Eng. Chem. Res. 28 (1989) 719–724.

4. a) A.V. Emeline, V.N. Kuznetsov, V.K. Ryabchuk, N. Serpone, Environ. Sci. Pollut. Res. Int. 19 (2012) 3666–3675. b) N. Serpone, A.V. Emeline, J. Phys. Chem. Lett. 3 (2012) 673–677.

5. J.C. Colmenares, R. Luque, J.M. Campelo, F. Colmenares, Z. Karpiński, A.A. Romero, Materials 2 (2009) 2228–2258.

6. Q. Xu, Y. Ma, J. Zhang, X.L. Wang, Z.C. Feng, C. Li, J. Catal. 278 (2011) 329–335.

7. J.T. Chang, Y.F. Lai, J.L. He, Surface Coating Technol. 200 (2005) 1640–1644.

8 A. Maldotti, A. Molinari, R. Amadelli, Chem. Rev. 102 (2002) 3811–3836.

9 X. Lang, W. Ma, C. Chen, H. Ji, J. Zhao, Acc. Chem. Res. 47 (2014) 355–363.

10 J. Zakzeski, P.C.A. Bruijnincx, A.L. Jongerius, B.M. Weckhuysen, Chem. Rev. 110 (2010) 3552–3599.

11 S. Yurdakal, G. Palmisano, V. Loddo, V. Augugliaro, L. Palmisano, J. Am. Chem. Soc. 130 (2008) 1568–1569.

12 S. Yurdakal, G. Palmisano, V. Loddo, O. Alagoz, V. Augugliaro, L. Palmisano, Green Chem. 13 (2009) 510–516.

14 C.J. Li, G.R. Xu, B.H. Zhang, J.R. Gong, Appl. Catal. B 115 (2012) 201–208.

13 T. Shishido, T. Miyatake, K. Teramura, Y. Hitomi, H. Yamashita, T. Tanaka, J. Phys. Chem. C 113 (2009) 18713–18718.

15 S.R. Kadam, V.R. Mate, R.P. Panmand, L.K. Nikam, M.V. Kulkarni, R.S. Sonawane, B.B. Kale, RSC Adv. 4 (2014) 60626–60635.

16 A. Tanaka, K. Hashimoto, H. Kominami, Chem. Commun. 47 (2011) 10446–10448.

17 Y. Zhang, N. Zhang, Z.R. Tang, Y.J. Xu, ACS Sustainable Chem. Eng. 1 (2013) 1258−1266.

18 W. Zhai, S. Xue, A. Zhu, Y. Luo, Y. Tian, ChemCatChem 3 (2011) 127–130.

19 M. Qamar, R.B. Elsayed, K.R. Alhooshani, M.I. Ahmed, D.W. Bahnemann, ACS Appl. Mater. Interfaces 7 (2015) 1257–1269.

20 L. Yuan, Q. Yu, Y. Zhang, Y.J. Xu, RSC Adv. 4 (2014) 15264–15270.

21 X. Dai, M. Xie, S. Meng, X. Fu, S. Chen, Appl. Catal. B 158 (2014) 382–390.

22 N. Zhang, Y. Zhang, X. Pan, X. Fu, S. Liu, Y.J. Xu, J. Phys. Chem. C 115 (2011) 23501–23511.

23 J.C. Colmenares, A. Magdziarz, O. Chernyayeva, D. Lisovytskiy, K. Kurzydlowski, J. Grzonka, ChemCatChem 5 (2013) 2270–2277.

24 J.C. Colmenares, A. Magdziarz, K. Kurzydlowski, J. Grzonka, O. Chernyayeva, D. Lisovytskiy, Appl. Catal. B 134–135 (2013) 136–144.

25 M. Ojeda, A. Pineda, A.A. Romero, V. Barron, R. Luque, ChemSusChem 7 (2014) 1876–1880.

26 J.C. Colmenares, P. Lisowski, D. Łomot, RSC Adv. 3 (2013) 20186–20192.

27 S. Sakthivel, H. Kisch, Angew. Chem. Int. Ed. 42 (2003) 4908–4911.

28 R. Cornell, U. Schertmann, Iron oxides in the laboratory: Preparation and characterization, VCH, Weinheim, 1991.

29 W. Choi, A. Termin, M.R. Hoffman, J. Phys. Chem. 98 (1994) 13669–13679.

30 K.B. Qi, B. Fei, J.H. Xin, Thin Solid Films 519 (2011) 2438–2444.

30 J.C. Colmenares, ChemSusChem 7 (2014) 1512–1527.1

32 a) Y. Ma, X.-T. Zhang, Z.-S. Guan, Y.-A. Cao, J.-N. Yao, J. Mater. Res. 16 (2001) 2928–2933; b) M. Litter, J. A. Navio, J. Photochem. Photobiol. A 98 (1996) 171–181.

33 Y. Shiraishi, T. Hirai, J. Photochem. Photobiol. C 9 (2008) 157–170.

34 A. Maldotti, A. Molinari, Top. Curr. Chem. 303 (2011) 185–216.

35 C.-J. Li, G.-R. Xu, B. Zhang, J.R. Gong, Appl. Catal. B 115–116 (2012) 201–208.

36 U. Stafford, K.A. Gray, P.V. Kamat, A. Varma, Chem. Phys. Lett. 205 (1993) 55–61.

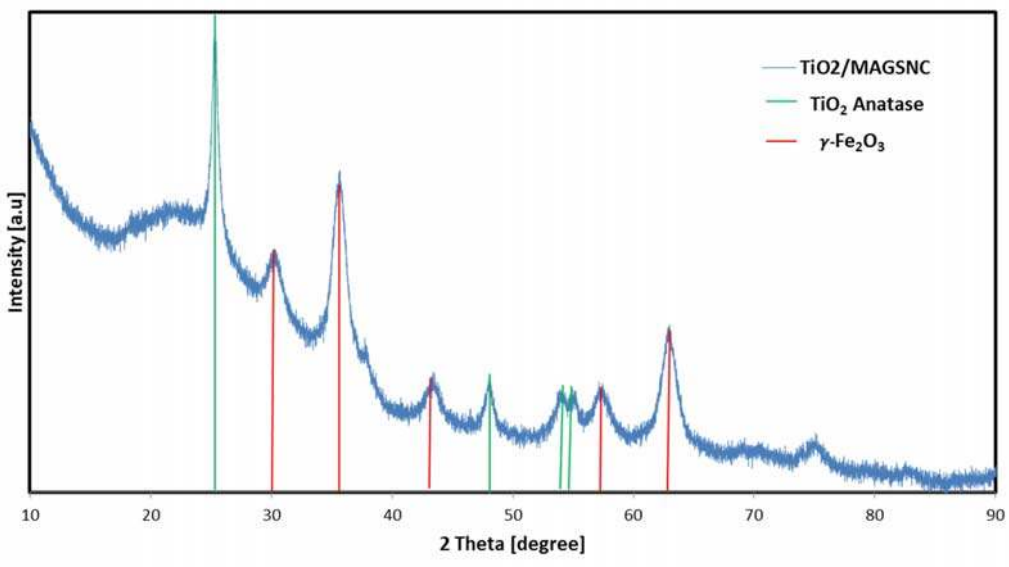

Figure 1. X-ray diffraction (XRD) pattern for TiO_2/MAGSNC

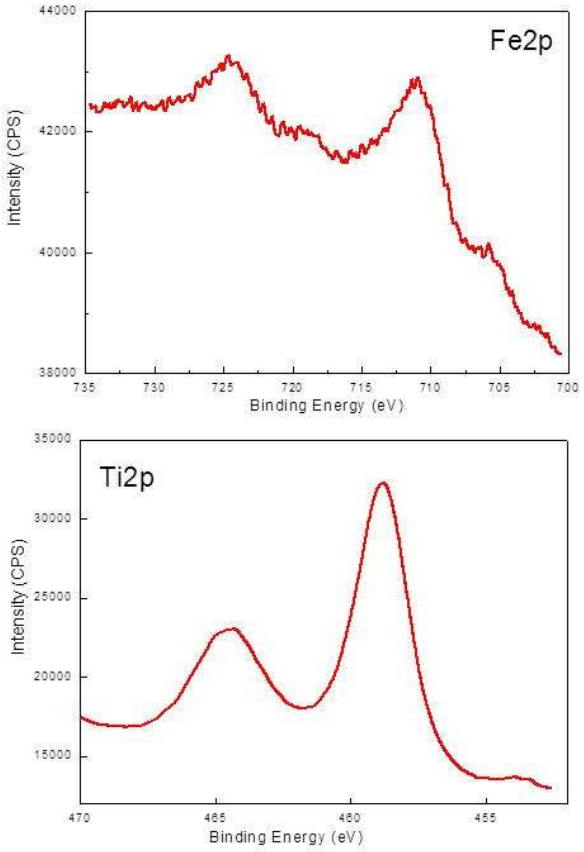

Figure 2. Fe2p and Ti2p XP spectra of TiO_2-MAGSNC.

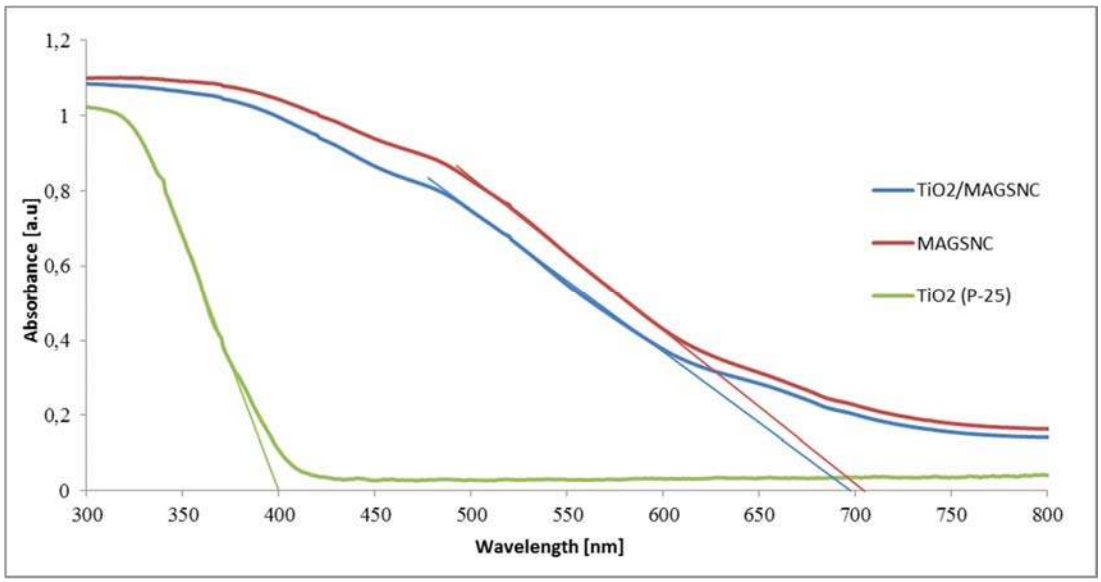

Figure 3. DR UV-Vis absorption spectra of MAGSNC, TiO_2/MAGSNC and TiO_2 Evonik P-25 catalysts.

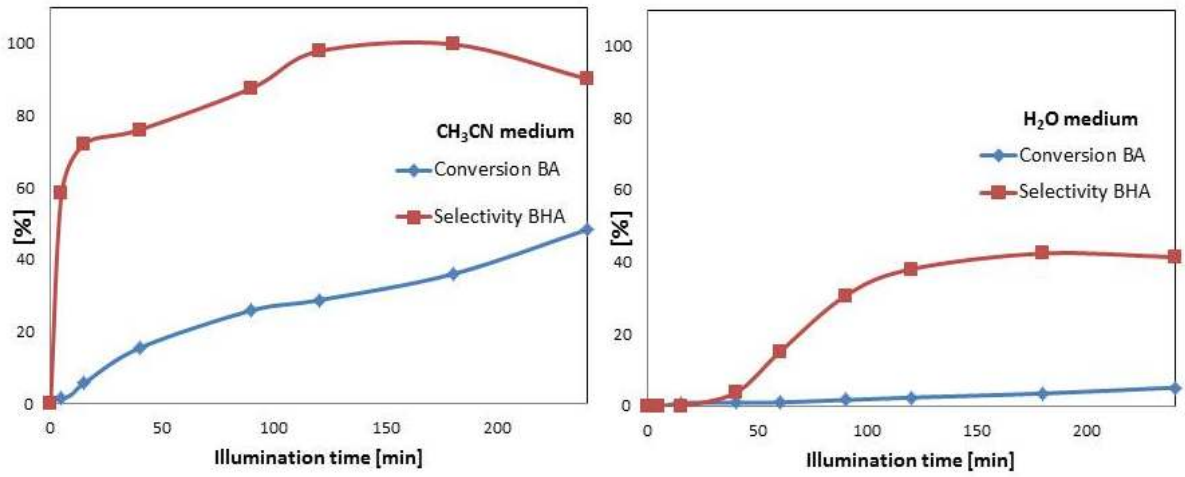

Figure 4. Conversion and selectivity results for the photo-oxidation of benzyl alcohol over TiO_2/MAGSNC. Reaction conditions: 150 mL of the mother solution, 1.5 mM of benzyl alcohol, 150 mg of the photocatalyst, 30 °C, 125 W UV lamp. BA: benzyl alcohol; BHA: benzaldehyde.

Table 1. Sumary of the textural and optical features of the photocatalysts.

	BET/BJH			UV-Vis	
Materials	S_{BET} ($m^2 g^{-1}$)	Pore Volume ($mL g^{-1}$)	Pore diameter (nm)	Band Gap (eV)	Absorption threshold (nm)
TiO_2/MAGSNC	292	0.31	4.60	1.78	696
MAGSNC	423	0.51	3.50	1.75	705
TiO_2 P-25	59	0.20	6.40	3.15	394

Table 2. Photocatalytic oxidation of benzyl alcohol using various photocatalytic nanomaterials.

Catalyst	**Solvent**	**Conversion (%)**	**Selectivity benzaldehyde (%)**	**Selectivity benzoic acid (%)**	**Yield BHA (%)**
Photolysis (no cat.)	CH_3CN	3	–	–	–
TiO_2/MAGSNC	**CH_3CN**	**50**	**90**	**–**	**47**
TiO_2/MAGSNC	H_2O	5	41	–	-
MAGSNC	CH_3CN	<5	–	–	–
TiO_2 (P-25)	CH_3CN	>99	32	6	33
TiO_2 (P-25)	H_2O	>99	8	0	7

Reaction conditions: initial benzyl alcohol concentration (C_0) = 1.5 mM, volume = 150 mL, catalyst loading = 1g/L. air flow rate = 25 mL/min, 125 W lamp, T = 30 °C, illumination time = 4 h. BA: benzyl alcohol; BHA: benzaldehyde; BAC: benzoic acid. The remaining selectivity to 100 corresponds mostly to CO_2.